Paper: ASAT-14-018-GU

14th International Conference on
AEROSPACE SCIENCES & AVIATION TECHNOLOGY,
ASAT - 14 – May 24 - 26, 2011, Email: asat@mtc.edu.eg
Military Technical College, Kobry Elkobbah, Cairo, Egypt
Tel: +(202) 24025292 –24036138, Fax: +(202) 22621908

Robust CLOS Guidance and Control: Part-2: Scalar H_∞ Autopilot Synthesis

A.N. Oda*, G.A. El-Sheikh†, M. Al-Ashry* and Y.Z. El-Halwagy*

Abstract: The great developments in applied mathematics and computational capabilities facilitate the design and implementation of robust control. In addition, the huge developments in nanotechnology and its availability in civilian level with less cost, size and weight attract many of the researchers allover the world towards embedded systems especially the embedded flight control. Among the real applications are the guided missiles especially the antitank guided missile systems which are commanded to the line of sight (CLOS) against ground and short range targets. The present work is concerned with improving the performance of an antitank guided missile system belonging to the first generation via robust synthesis of autopilot and guidance systems. The design and analysis necessitates somehow accurate model with different uncertainties (objective of Part-1 of the paper) for the system, a robust autopilot design (objective of Part-2 of the paper) and implementation via hardware in the loop (HIL) simulation (objective of Part-3 of the paper).

This part of the paper is devoted to the derivation of the missile-control system transfer functions representing the system dynamics in pitch plane based on the designed 6DOF simulation model in Part-1 of the paper. These transfer functions are augmented with mathematical formulation for the system uncertainty to be considered during the robust (H_∞) design. Then, it presents the results of 6DOF simulation with justification and validation against previous work. The next objective for this part is the autopilot design using H_∞ technique with justification against previous work and reference flight data concerning the performance requirements of time responses and flight path characteristics. The new design is implemented within the 6DOF simulation from which the obtained results clarify its capability to stabilize the system in presence of un-modeled dynamics and satisfy the performance requirements with disturbance rejection and measurement noise attenuation. However, the selection of the weighting functions necessary for the H_∞ design is cumbersome and necessitates more investigation to stay on some rules of thumb as guidelines to subsequent research. Towards this objective the next part of the paper is a first trial via conducting the simulation with some hardware (pitch and yaw) in the loop.

Keywords: Command Guidance Systems, Robust Control, Uncertainties

1. Introduction

The ever-increasing development of tanks capabilities necessitates the design of accurate control and guidance system for an antitank missile in presence of disturbance, measurement noise, and un-modelled dynamics. To achieve this objective, the first part of this paper [17]

* Egyptian Armed Forces, Egypt
† Professor, , gaelsheikh@gmail.com, Tel. 02,01002682402

extracted a nonlinear mathematical model representing the dynamical behaviour of the underlying missile for different flight phases with uncertainty quantification. The system uncertainties included thrust variation due to different causes, variation in aerodynamic coefficients and parameters, wind velocity in different directions and different trim conditions. To overcome different sources of uncertainty, robust control is used to design the autopilot such that the system is stable with the ability to overcome un-modelled dynamics, to reject the disturbances and minimize the effects of measurement noises overall the missile flight envelope. The performance specifications include overshoot, speed of response, steady state error, and system stability in addition to flight paths with different engagement scenarios. To overcome the effects due to uncertainties and achieve the performance requirements this paper is devoted to design a robust guidance and control for the underlying command to line-of-sight (CLOS) system using the H_∞ with evaluation. This control system is said to be robust when it maintains a satisfactory level of stability and performance over a range of plant parameters, disturbances and noises [7]. Thus, the objective is to investigate the robustness of the designed autopilot against uncertainties due to different sources. The designed controller is implemented within the missile control system and should be insensitive to model uncertainties and be able to suppress disturbances and noise over the whole envelope of operation to prove its robustness. This paper is devoted to the autopilot design including the jetevator control using the H_∞ in state space form and its implementation for guidance and control performance analysis.

A feedback-control system must satisfy certain performance specifications and it must tolerate model uncertainties. The feedback control system has three components: the plant, sensors to

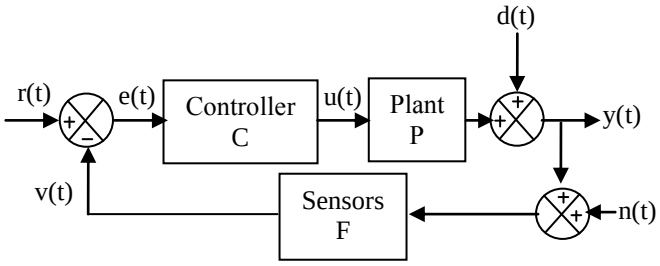

Fig. 1 Feedback Control

measure the plant outputs, and a controller to generate the plant's input or control signal [5], Fig. 1. Generally, this system has three inputs that contribute to three outputs [the actual output *y(t),* the tracking error $e(t)$, and the controller/ actuator signal, *u(t)*] as described by

$$\begin{bmatrix} y \\ u \\ e \end{bmatrix} = \begin{bmatrix} T/F & S & -T \\ R & -RF & -RF \\ S & -FS & -FS \end{bmatrix} \begin{bmatrix} r \\ d \\ n \end{bmatrix} \tag{1a}$$

where the sensitivity function (S), the complementary sensitivity function (T) and the control sensitivity function *(R)* are defined as [8]

$$S = \frac{1}{1+L},\ T = \frac{L}{1+L},\ R = \frac{C}{1+L} \tag{1b}$$

Where, L denotes the loop transfer function (L=FPC) and (T=1-S).

2. Robust Control

One way to describe the performance of a control system is in terms of the size of certain signals of interest. For example, the performance of a tracking system could be measured by the size of the error signal. There are several ways of defining a signal's size (i.e. several norms for signals), among these norms is the ∞-Norm. The ∞-Norm of a signal u(t) is the

least upper bound of its absolute value $\|u\|_\infty := \sup_t |u(t)|$. There are several robust techniques, among them is the H_∞ where a quantitative measure for the size of the system uncertainty is considered. The infinity norm of the transfer function relating the input to the output is the worst-case gain between the two, where both the input and output are measured either by their energy or peak value [4]. Other measures of gain can also characterize worst-case amplifications, but in ways which seem to be less useful in practice.

The set of all stable transfer functions whose infinity norms are finite forms a *Hardy space* [2, 3, 4] and denoted by $\|H\|_\infty$. Moreover, it is the approach which gives much of recent robust control theory its name. The theory is of great interest because it gives solutions to realistic robust control problems known as $\|H\|_\infty$ optimization problems. One would expect it to be harder than LQG theory, because *min-max* optimization problems are usually harder than quadratic ones, but in fact recent developments have shown the theory to have remarkable similarities with the LQG theory, and LQG problems can even seen as special cases of $\|H\|_\infty$ problems. In addition to the theoretical advances, one should add that a major reason why this theory is of practical interest is the availability of low-cost interactive software, like MATLAB, which makes it possible to perform all the necessary computations quickly and easily.

2.1 Types of Uncertainties

No mathematical system can precisely model a real physical system; there is always uncertainty and we cannot predict exactly what the output of the system will be even if we know the input [3]. The real problem in robust control system design is to synthesize a control law which maintains system response and error signals to be within pre-specified tolerances despite the effects of uncertainties. Uncertainty may take many forms among them are the noise/disturbance signals and transfer function modeling errors in addition to un-modeled nonlinear distortion. Consequently, it had adopted a standard quantitative measure for the size of the uncertainty using H_∞ norm, as shown in Fig. 2 [1,3,14]. The model error Δ can be represented by an unknown transfer function that indicates the difference between the actual process and the model. This general setup allows a control system designer to capture all these uncertainties, both structured and unstructured, and formulate them into the design. There are two types of uncertainty defined in robust control and known as *unstructured* and *structured* [11,14].

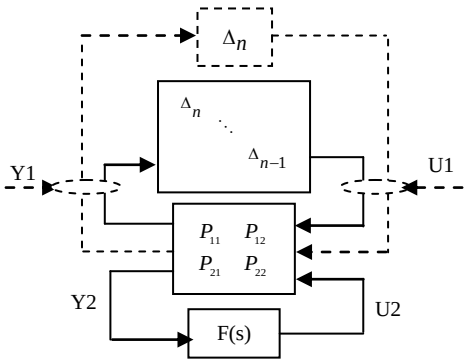

Fig. 2: Canonical Robust Control Problem

2.2 H_∞ Control Theory

The methods of H_∞ synthesis are powerful tools for designing robust feedback control systems to achieve singular value loop shaping specifications. The *standard* H_∞ *control problem* is sometimes also called the H_∞ *small gain problem*. The small-gain theorem states that if *a feedback loop consists of stable systems, and the product of all their gains is smaller*

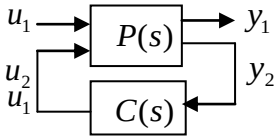

Fig. 3: Small Gain Problem

than one, then the feedback loop is stable [1,7,19]. That is, assuming that the blocks P and C in Fig. 3 are stable, then the closed loop system remains stable if $\|T_{y_1u_1}\| < 1$, where $\|T_{y_1u_1}\|$ is the feedback closed loop transfer function. The small gain problem shows a general setup, and the problem of making $\|T_{y_1u_1}\|_\infty \le 1$ is also called the *small-gain problem*.

For H_∞ design problem, the state-space model of an augmented plant $P(s)$ with weighting functions $W_p(s)$, $W_u(s)$, and $W_t(s)$ which penalize the error signal, control signal and output signal, respectively, is formulated as shown in Fig. 4 so that the closed-loop transfer function matrix is the weighted mixed sensitivity;

$$T_{y1u1} = \begin{bmatrix} W_p S \\ W_u R \\ W_t T \end{bmatrix} \tag{2}$$

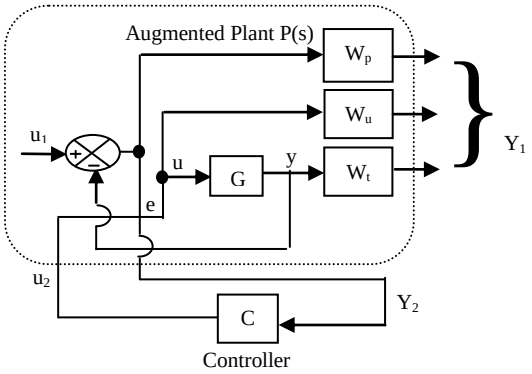

Fig. 4 Augmented Plant $P(s)$

In practice, it is usually not necessary to obtain a true optimal controller, but it is often simpler to find a sub-optimal controller. Suppose that $\gamma_{\min}$ is the minimum value of $\|F_i(P,C)\|_\infty$ over all possible stabilizing controllers C. Then, the H_∞ sub-optimal control problem is:

Given a $\gamma > \gamma_{\min}$, find all stabilizing controllers such that $\|F_i(P,C)\|_\infty < \gamma$.

This problem can be solved efficiently using the algorithm of Doyle et al. (1989), by reducing γ iteratively to yield the optimal solution [5].

2.3 Controller Performance Evaluation

Considering the feedback control system shown in Fig. 1, the stability margins and performance of such systems can be quantified using the singular values of the closed-loop transfer function matrices from r to each of the three outputs e, u, and y as defined in Eq^{n} 1

and 2. The singular value bode plot of each of the three transfer functions S(s), R(s), and T(s) play an important role in robust control system design. Considering the augmented plant shown in Fig. 4, the singular values of $S(j\omega)$ determine the disturbance attenuation, because S(s) is the closed-loop transfer function from disturbance (d) to the plant output (y). Thus disturbance attenuation performance specification can be written as:

$$\bar{\sigma}\{S(j\omega)\} \le \left|W_p^{-1}(j\omega)\right| \tag{3}$$

where $\left|W_p^{-1}(j\omega)\right|$ is the desired disturbance attenuation factor. Allowing $\left|W_p(j\omega)\right|$ to depend on frequency ω enables you to specify a different attenuation factor for each frequency ω. The singular value Bode plot of R(s) and of T(s) are used to measure the stability margins of feedback designs in the face of additive plant perturbations Δ_A and multiplicative plant perturbations Δ_M, respectively. The singular value Bode plot of complementary sensitivity T(s) determines the stability margin for multiplicative perturbation Δ_M, where the multiplicative stability margin is the 'size' of the smallest stable $\Delta_M(s)$ that destabilizes the system when $\Delta_A = 0$.

Multiplicative robustness: Taking $\bar{\sigma}\{\Delta_M(j\omega)\}$ to be the 'size' of $\Delta_M(j\omega)$, the 'multiplicative' stability robustness is characterized by the size of the smallest destabilizing multiplicative uncertainty $\Delta_M(s)$ as

$$\bar{\sigma}\{\Delta_M(j\omega)\} \le \left|\frac{1}{\bar{\sigma}\{T(j\omega)\}}\right| \tag{4}$$

The smaller is $\bar{\sigma}\{T(j\omega)\}$, the greater will be the size of the smallest destabilizing multiplicative perturbation and hence the greater will be the stability margin.

Additive robustness: taking $\bar{\sigma}\{\Delta_A(j\omega)\}$ to be the definition of the 'size' of $\Delta_A(j\omega)$ at frequency ω, the size of the smallest destabilizing additive uncertainty $\Delta_A(s)$ is

$$\bar{\sigma}\{\Delta_A(j\omega)\} \le \left|\frac{1}{\bar{\sigma}\{R(j\omega)\}}\right| \tag{5}$$

As a consequence of robustness Eq^{n} 4 and 5, it is common to specify the stability margin of the control system via singular value inequalities such as:

$$\begin{aligned} \bar{\sigma}\{R(j\omega)\} &\le \left|W_u^{-1}(j\omega)\right| \\ \bar{\sigma}\{T(j\omega)\} &\le \left|W_t^{-1}(j\omega)\right| \end{aligned} \tag{6}$$

where $\left|W_u(j\omega)\right|$ and $\left|W_t(j\omega)\right|$ are the respective sizes of the largest anticipated additive and multiplicative plant perturbations. It is common practice to lump the effects of all plant uncertainty into a single fictitious multiplicative perturbation Δ_M, so that the control design requirements can be written in the form: $\frac{1}{\bar{\sigma}_i\{S(j\omega)\}} \ge \left|W_p(j\omega)\right|$ and $\bar{\sigma}_i(T(j\omega)) \le \left|W_t^{-1}(j\omega)\right|$.

In addition, the following trade-offs should be exercised: good command following and disturbance rejection necessitates L to be large while good noise attenuation and robust stability necessitates L to be small. That is, compromise between conflicting requirements should be experienced.

2.4 Model Order Reduction

The robust controller's design for complex systems necessitates model reduction to simplify the obtained controller to a reasonable order. The order reduction can be carried to the original system, to the obtained controller or to the system as whole. In this work a good

model reduction algorithm (based on Hankel singular values) is applied to the control law (designed controller) to reduce its complexity with little change in control system performance. Eigenvalues define system stability whereas Hankel singular values define the energy of each state in the system [10]. Thus, keeping larger energy states of the system preserves most of its characteristics in terms of stability, frequency, and time responses. Therefore, for a given stable state-space system (A,B,C,D) the Hankel singular values are defined as follows:

$$\sigma_H = \sqrt{\lambda_i(PQ)} \tag{7a}$$

where P and Q are controllability and observability grammians satisfying the following equations:

$$\begin{aligned} AP + PA^T &= -BB^T \\ A^TQ + QA &= -C^TC \end{aligned} \tag{7b}$$

There are several algorithms for model approximation and order reduction that can be used to control the absolute or relative approximation error based on the Hankel singular values of the system [10,14]. Generally, model order reduction approaches can be put into two categories:
Additive error method in which the reduced-order model G_{red} has an additive error bounded by the $\|G - G_{red}\|_\infty$ error criterion.
Multiplicative error method where the reduced-order model has a multiplicative or relative error bounded by the $\|G^{-1}(G - G_{red})\|_\infty$ error criterion.

The error is measured in terms of peak gain across frequency (H_∞ norm), and the error bounds are functions of the neglected Hankel singular values.

3. Problem Formulation

Towards the autopilot design, the guidance equations [17] have to be linearized for extracting the necessary transfer function or state space models. That is, consider equations which describe equations of motion for the intended guided missile, with the assumptions [4,6,9,15]: pitch motion, constant velocity, neglect g, small firing angles (α, β), and small thrust jetivator angles δ_{jp} and δ_{jy} such that $F_{Tx_1} = F_{T_1}$, $F_{Ty_1} = -F_{T_1}\delta_{jy}$, and $F_{Tz_1} = -F_{T_1}\delta_{jp}$.

3.1 Pitch Jetivator and Airframe Dynamics

The performance of the underlying system is measured through the minimum miss distance and its capability to overcome different sources of uncertainty and achieve the missile interception with its target. The guidance process is devoted to correct the missile trajectory through its flight and to overcome the external and internal error sources. Toward this objective the guidance equations have to be linearized and yield the airframe transfer function that can be used for robust autopilot design and analysis. A simple method for selecting weight functions for the H_∞ control technique is followed by considering the plant P(s) as the actuator cascaded by the missile airframe augmented with the two weighting functions w_p which penalizes error signal (e) and w_t that penalizes the output (y). The equations describing dynamics of the guided missile c.g motion, rotation around c.g. and geometrical relations can be summarized as follows:

$$\begin{aligned} \ddot{\theta} &= M_{y1\alpha}\alpha + M_{y1\dot{\theta}}\dot{\theta} + M_{\delta_{jp}}\delta_{jp} \\ \dot{\vartheta} &= n_\alpha\alpha + n_{\delta_{jp}}\delta_{jp} \qquad\qquad \dot{\alpha} = -n_\alpha\alpha - n_{\delta_{jp}}\delta_{jp} + \dot{\theta} \\ \vartheta &= \theta - \alpha \end{aligned} \tag{8}$$

with $M_{y1\alpha} = m_{y1}^{\alpha} sql_y / I_{yy}$, $M_{y1\dot{\theta}} = m_{y1}^{\omega_{y1}} sql_y / I_{yy}$, $M_{\delta_{jp}} = -F_{T_1} \times l_t / I_{yy}$, $n_{\delta_{jp}} = \frac{F_{T_1}}{mv_M}$, $n_\alpha = \frac{1}{mv_M}(C_z^{\alpha} sq + F_{T_1})$

where S represents the characteristic area, (q) represents the dynamic pressure given by $q = 0.5\rho(v_b)^2$ [Kg/m/sec^2], ρ air density [kg/m^3], and v_b is the missile velocity in BCS. As a consequence of algebraic manipulation to Eq^{n} 8 the obtained airframe transfer functions are considered as:

$$\frac{\dot{\theta}(s)}{\delta_{jp}(s)} = \frac{M_{\delta_{jp}} s + (M_{\delta_{jp}} n_\alpha - M_{y1\alpha} n_{\delta_{jp}})}{s^2 + (n_\alpha - M_{y1\dot{\theta}})s - (M_{y1\dot{\theta}} n_\alpha + M_{y1\alpha})}, \quad \text{Body Rate Transfer Function} \tag{9a}$$

$$\frac{\alpha(s)}{\delta_{jp}(s)} = \frac{-s n_{\delta_{jp}} + M_{\delta_{jp}} + M_{y1\dot{\theta}} n_{\delta_{jp}}}{(s^2 - s(M_{y1\dot{\theta}} - n_\alpha) - (M_{y1\dot{\theta}} n_\alpha + M_{y1\alpha})}, \quad \text{Angle of Attack Transfer Function} \tag{9b}$$

$$\frac{\dot{\vartheta}(s)}{\delta_{jp}(s)} = \frac{n_{\delta_{jp}} s^2 - M_{y1\dot{\theta}} n_{\delta_{jp}} s - n_{\delta_{jp}} M_{y1\alpha} + n_\alpha M_{\delta_{jp}}}{s^2 - s(M_{y1\dot{\theta}} + n_\alpha) + M_{y1\dot{\theta}} n_\alpha + M_{y1\alpha}}, \quad \text{Flight Path Transfer Function} \tag{9c}$$

$$\frac{J_z(s)}{\delta_{jp}(s)} = -V_M \left(\frac{n_{\delta_{jp}} s^2 - M_{y1\dot{\theta}} n_{\delta_{jp}} s - n_{\delta_{jp}} M_{y1\alpha} + n_\alpha M_{\delta_{jp}}}{s^2 - s(M_{y1\dot{\theta}} + n_\alpha) + M_{y1\dot{\theta}} n_\alpha + M_{y1\alpha}} \right), \quad \text{Normal Acceleration Transfer Function} \tag{9d}$$

The pitch control system structure is shown in Fig. 5, where the gyro is a free gyro used to measure the body pitch angle. The airframe transfer function (θ/δ_{jp}) expressed in Eq^{n} 9 is obtained via conducting the 6DOF simulation with target at distance 500 [m] and considering 10 operating points during the flight envelope. The extracted airframe transfer function has the form $\frac{\theta(s)}{\delta_{jp}(s)} = \frac{a_1 s^2 + a_2 s + a_3}{s^3 + b_1 s^2 + b_2 s}$. The frequency response of the airframe at different operating conditions is shown in Fig. 6 which clarifies that the max gain variation is 53.9 [dB] at low frequency and 26.2 [dB] at high frequency. In addition, the maximum phase variation is 22.5 [deg] at low frequency and 80 [deg] at high frequency.

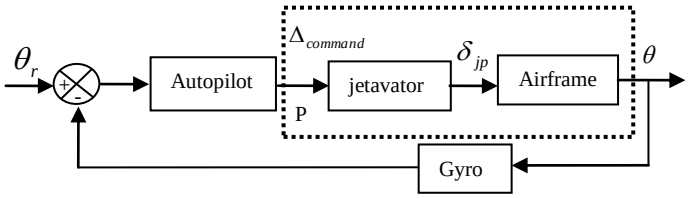

Fig. 5 Pitch control system

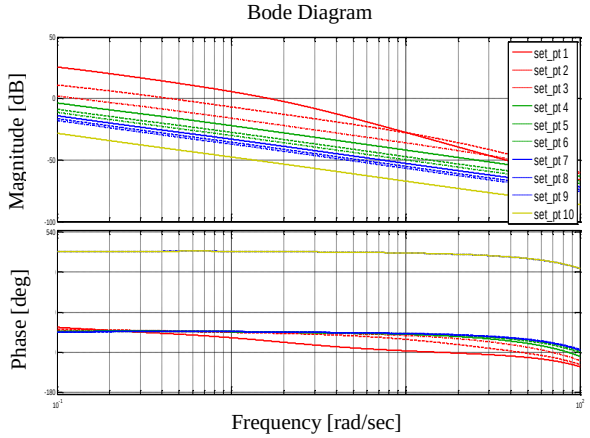

Fig. 6: Bode Diagram of airframe (θ/δ_{jp})

3.2 Pitch Airframe-Jetivator with Uncertainty Modelling

The main variation of coefficients for perturbed motion happens in the aerodynamics coefficients $C_x, C_y^{\alpha}, m_z^{\alpha}, m_z^{\omega_z}$ which are usually determined experimentally as functions of the Mach number that may vary in sufficiently wide intervals. Thus, the aerodynamic coefficients are supposed to exercise about 25 % variations in the perturbed motion and this level of uncertainty will be useful for justifying the robustness of the designed controller. In deriving the uncertain model of the system dynamics the angle ϑ is eliminated by using the relationship $\vartheta = \theta - \alpha$ (Eq^{n} 8) which allows to avoid the use of the angle θ itself and works only with its derivatives $\dot{\theta}$ and $\ddot{\theta}$. This in turn makes it possible to avoid the usage of an additional integrator in the plant dynamics that violates the conditions for controller existence in the H_∞ design. The five uncertain coefficients of the perturbed motion equations are $M_{y1\alpha}$, $M_{y1\dot{\theta}}$, $M_{\delta_{jp}}$, n_α and $n_{\delta_{jp}}$ with about 25% for each. Each uncertain coefficient (c) may be represented in the form $c = \bar{c}(1 + P_c\delta_c)$ where c is the nominal value of the coefficient $\bar{c}$ (at a given time instant), p_c is the relative uncertainty (p_c=0.3 for uncertainty 25%) and $-1 \le \delta_c \le 1$. The uncertain coefficient may be further represented as an upper linear fractional transformation (LFT) [4] in δ_c: $c = F_u(M_c, \delta_c)$ where $M_c = \begin{bmatrix} 0 & \bar{c} \\ p_c & \bar{c} \end{bmatrix}$ as is shown in Fig. 7.

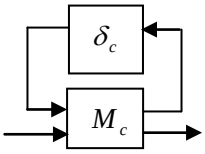

Fig. 7: LFT uncertain plant

The uncertainty model corresponding to the system of Eq^{n} 8 is difficult to be obtained directly. That is why the uncertain model is derived corresponding to its individual equations and combining them in a common model. Consider the equation ($\dot{\alpha} = -n_\alpha\alpha - n_{\delta_{jp}}\delta_{jp} + \dot{\theta}$) for which the uncertain model is shown in Fig. 8a, where $n_\alpha = \begin{bmatrix} 0 & \bar{n}_\alpha \\ p_\alpha & \bar{n}_\alpha \end{bmatrix}$, $n_{\delta_{jp}} = \begin{bmatrix} 0 & \bar{n}_{\delta_{jp}} \\ p_{jp} & n_{\delta_{jp}} \end{bmatrix}$, p_α=0.3, p_{jp}=0.25, $|\delta_{n_\alpha}| \le 1, |\delta_{n_{\delta_{jp}}}| \le 1$ and the nominal values of the coefficients are denoted by bar. The uncertain model corresponding to the equation ($\ddot{\theta} = M_{y1\alpha}\alpha + M_{y1\dot{\theta}}\dot{\theta} + M_{\delta_{jp}}\delta_{jp}$) is shown in Fig. 8b, where $M_{y1\alpha} = \begin{bmatrix} 0 & \bar{M}_{y1\alpha} \\ p_{y1\alpha} & \bar{M}_{y1\alpha} \end{bmatrix}$, $M_{y1\dot{\theta}} = \begin{bmatrix} 0 & \bar{M}_{y1\dot{\theta}} \\ p_{y1\dot{\theta}} & \bar{M}_{y1\dot{\theta}} \end{bmatrix}$, $M_{\delta_{jp}} = \begin{bmatrix} 0 & \bar{M}_{\delta_{jp}} \\ p_{\delta_{jp}} & \bar{M}_{\delta_{jp}} \end{bmatrix}$, $p_{y1\alpha}$=0.3, $p_{y1\dot{\theta}}$=0.3, $p_{\delta_{jp}}$=0.3, $|\delta_{M_{y1\alpha}}| \le 1, |\delta_{M_{y1\dot{\theta}}}| \le 1, |\delta_{M_{jp}}| \le 1$ and the nominal values of coefficients are denoted by bar.

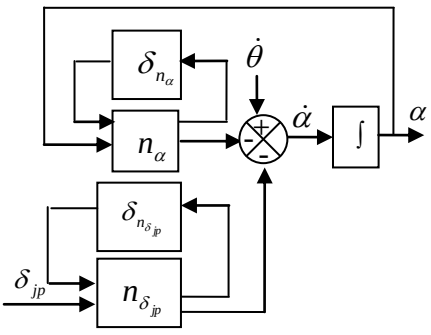

Fig. 8a: Uncertain model for α

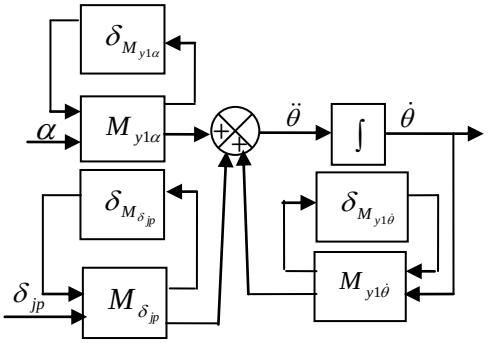

Fig. 8b: Uncertain model for θ

Pulling out the uncertain parameters from the known part of the model yields uncertain model in the form of upper LFT [12,16,18] as shown in Fig. 9 with a 5×5 matrix Δ of uncertain parameters, i.e. $\Delta = diag(\delta_{n_\alpha}, \delta_{n_{\delta_{jp}}}, \delta_{M_{y1\alpha}}, \delta_{M_{\delta_{jp}}}, \delta_{M_{y1\dot{\theta}}})$. Due to the complexity of the plant, the easiest way in simulation and design is to define the uncertainty model and implement the interconnection system, where the plant input is considered as the reference signal u(t) to the fins servo-actuator, and the plant output is the body angle θ. The equations describing dynamics of guided missile c.g motion, rotation around its c.g and geometrical relations are shown in Eq^{n} 9. Consequently, the block diagram describing the pitch stabilization system can be depicted as shown in Fig. 10. The extracted transfer function has the form $\frac{\theta}{\Delta_{p_{command}}} = \frac{a_1 s^4 + a_2 s^3 + a_3 s^2 + a_4 s + a_5}{s^5 + b_1 s^4 + b_2 s^3 + b_3 s^2 + b_4 s + b_5}$, the coefficients of which are obtained by conducting the 6DOF simulation with a target at range 500[m] and the flight envelope is divided into 10 operating points. The frequency response of the pitch airframe jetivator is shown in Fig. 11 for the 10 operating points. This figure clarifies maximum gain variation of about 53.3 [dB] and phase variation of about 387.5 [deg].

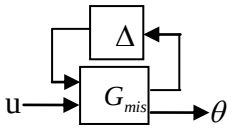

Fig. 9: Upper LFT Plant model

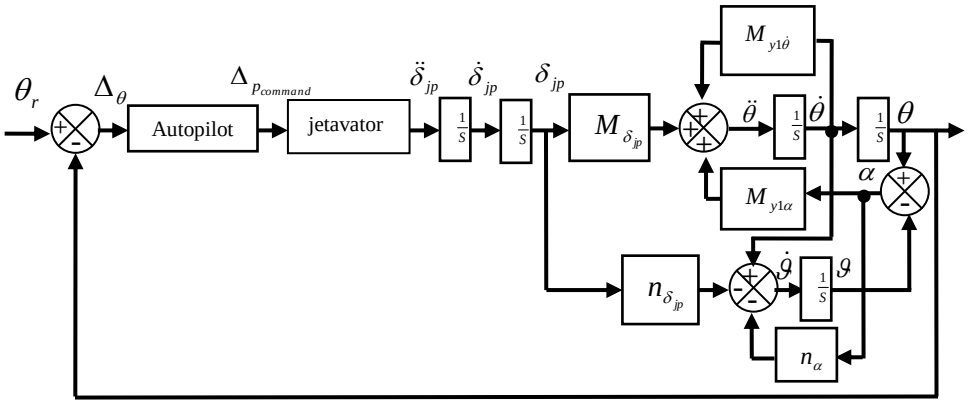

Fig. 10: Pitch stabilization system

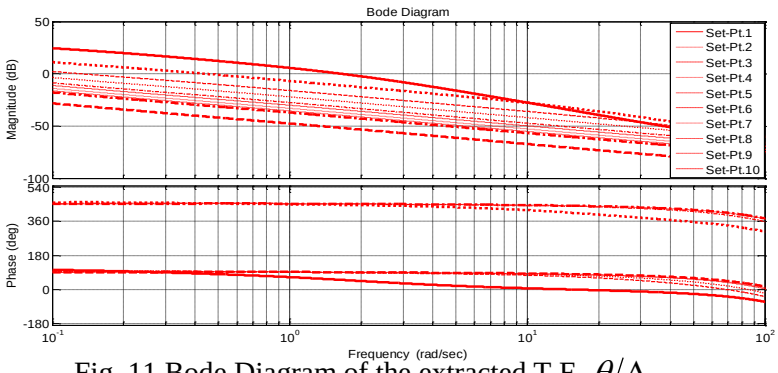

Fig. 11 Bode Diagram of the extracted T.F. $\theta/\Delta_{command}$

4. Robust Autopilot Synthesis

4.1 Nominal Pitch Channel Modeling

Let us consider either the 6th pitch airframe transfer function or the 4th one as a nominal airframe which have a moderate frequency response compared with the remainder trim points, then find the overall plant transfer function which is the jetivator ($\delta_{jp}/\Delta_{P_{command}}$) cascaded with the airframe (θ/δ_{jp}) as shown in Fig. 10. The Jetivator transfer function has the form [13]:

$$\frac{\delta_{jp}}{\Delta_{P_{command}}} = \frac{2.85}{6.33\times10^{-5}s^2 + 0.0079s + 1}$$

Case-A: The 6th pitch airframe transfer function is considered and thus the overall plant transfer function is

$$\frac{\theta}{\Delta_{P_{command}}} = \frac{1.024\times10^{-8}s^2 - 1.362\times10^{5}s - 5.385\times10^{4}}{s^5 + 392.6s^4 + 4.934\times10^{4}s^3 + 4.246\times10^{6}s^2 + 1.959\times10^{6}s} \tag{10}$$

Case-B: The 4th pitch airframe transfer function is considered and yields the overall plant transfer function is

$$\frac{\theta}{\Delta_{P_{command}}} = \frac{2.559\times10^{-9}s^2 - 1.387\times10^{5}s - 3.342\times10^{4}}{s^5 + 234.1s^4 + 2.947\times10^{4}s^3 + 1.731\times10^{6}s^2 + 5.179\times10^{5}s} \tag{11}$$

4.2 Autopilot Design using H_∞ Loop Shaping

This approach is utilized for the autopilot design without uncertainty modelling i.e. there is no certain structure for the uncertainty during the design.

4.2.1 Autopilot Design trials

Let us consider the following weights:

$$W_p = \frac{0.1s + 1.5}{s + 0.015},\quad W_t = \frac{10s + 15}{1.9s + 5} \tag{12}$$

$$W_p = \frac{0.1s + 1.5}{s + 0.015},\quad W_t = \frac{2s + 3}{1.9s + 5} \tag{13}$$

$$W_p = \frac{0.1s + 1.5}{s + 0.015},\quad W_t = \frac{3.5s + 2.9954}{1.9s + 5} \tag{14}$$

Trial-1: Considering the nominal plant Case-A, the weights (12) and the optimal H_∞ robust control yield the controller C_{A1} as:

$$C_{A1} = \frac{2.867\times10^{5}s^6 + 1.133\times10^{8}s^5 + 1.444\times10^{10}s^4 + 1.255\times10^{12}s^3 + 3.765\times10^{12}s^2 + 1.478\times10^{12}s + 143.3}{s^7 + 612.4s^6 + 1.553\times10^{5}s^5 + 2.327\times10^{7}s^4 + 1.994\times10^{9}s^3 + 3.272\times10^{10}s^2 + 1.311\times10^{10}s + 1.892\times10^{8}}$$

The frequency response of sensitivities and weights are shown in Fig. 12a, b, c and the closed loop step response using the obtained controller is shown in Fig. 12d.

Trial-2: Considering the nominal plant Case-A, the weights (13) and the optimal H_∞ robust control yield the controller C_{A2} as:

$$C_{A2} = \frac{8.628\times10^{6}s^6 + 3.41\times10^{9}s^5 + 4.346\times10^{11}s^4 + 3.776\times10^{13}s^3 + 1.133\times10^{14}s^2 + 4.448\times10^{13}s + 2189}{s^7 + 1063s^6 + 5.178\times10^{5}s^5 + 1.494\times10^{8}s^4 + 2.544\times10^{10}s^3 + 6.925\times10^{11}s^2 + 2.801\times10^{11}s + 4.045\times10^{9}}$$

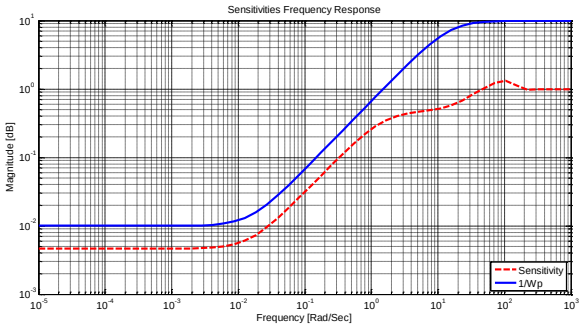

Fig. 12a: Sensitivity and output weighting inverse

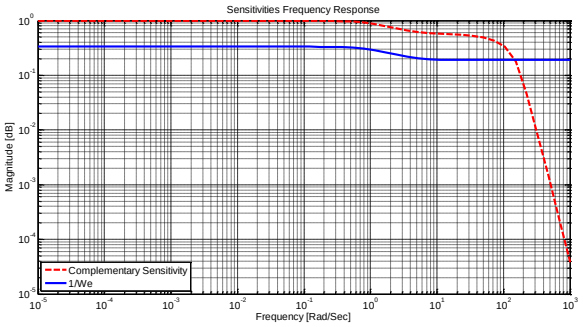

Fig. 12b: Complementary and error weighting inverse

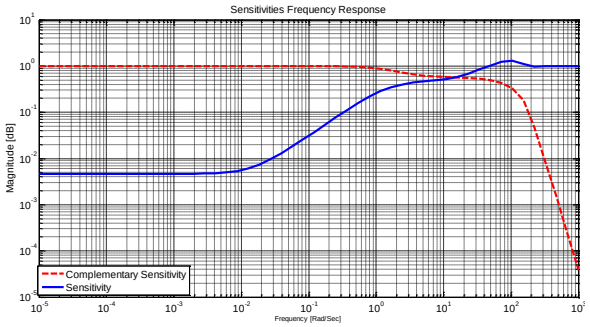

Fig. 12c: Sensitivity and Complementary weighting

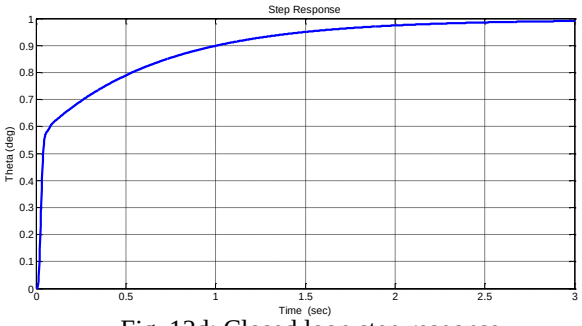

Fig. 12d: Closed loop step response

Trial-3: Considering the nominal plant Case-A, the weights (14) and the optimal H_∞ robust control yield the controller C_{A3} as:

$$C_{A3} = \frac{1.237\times10^{7}s^{6} + 4.888\times10^{9}s^{5} + 6.23\times10^{11}s^{4} + 5.412\times10^{13}s^{3} + 1.624\times10^{14}s^{2} + 6.376\times10^{13}s + 5103}{s^{7} + 1200s^{6} + 6.681\times10^{5}s^{5} + 2.211\times10^{8}s^{4} + 4.314\times10^{10}s^{3} + 1.932\times10^{12}s^{2} + 7.86\times10^{11}s + 1.136\times10^{10}}$$

Trial-4: Considering the nominal plant Case-B, the weights (12) and the optimal H_∞ robust control yield the controller C_{B1} as:

$$C_{B1} = \frac{2.403\times10^{5}s^{6} + 5.69\times10^{7}s^{5} + 7.231\times10^{9}s^{4} + 4.347\times10^{11}s^{3} + 1.219\times10^{12}s^{2} + 3.276\times10^{11}s + 31.43}{s^{7} + 507.7s^{6} + 1.278\times10^{5}s^{5} + 1.94\times10^{7}s^{4} + 1.701\times10^{9}s^{3} + 2.767\times10^{10}s^{2} + 6.978\times10^{9}s + 9.842\times10^{7}}$$

Trial-5: Considering the nominal plant Case-B, the weights (13) and the optimal H_∞ robust control yield the controller C_{B2} as:

$$C_{B2} = \frac{1.906\times10^{6}s^{6} + 4.513\times10^{8}s^{5} + 5.735\times10^{10}s^{4} + 3.448\times10^{12}s^{3} + 9.671\times10^{12}s^{2} + 2.598\times10^{12}s + 187.7}{s^{7} + 833.3s^{6} + 2.874\times10^{5}s^{5} + 5.84\times10^{7}s^{4} + 7.151\times10^{9}s^{3} + 1.568\times10^{11}s^{2} + 3.969\times10^{10}s + 5.601\times10^{8}}$$

The results obtained from these design trials can be summarized in following Table:

Trial Number	Obtained controller	Rise Time	Settling time	$\|\omega_p S\|_\infty$	$\|\omega_t T\|_\infty$
1	C_A1	0.99	2.21	0.4635	3.0008
2	C_A2	0.756	1.79	0.3297	0.6786
3	C_A3	1.36	2.91	0.6438	0.8713
4	C_B1	0.99	2.21	0.4635	3.0008
5	C_B2	0.752	1.79	0.3330	0.6810

The results clarify that the weights (13, 14) yield designs with $\|W_p S\|_\infty$ and $\|W_t T\|_\infty$ <1 and the closed loop step response has settling and rise times smaller than that obtained from another

controller obtained using the weights (12) which yields that $\|W_p S\|_\infty$ <1 and $\|W_t T\|_\infty$ >1. In addition, the angle of departure between sensitivity and complementary weighting functions in the first case with $\|W_p S\|_\infty$ and $\|W_t T\|_\infty$ <1 is greater than those obtained in the second case where $\|W_p S\|_\infty$ <1 and $\|W_t T\|_\infty$ >1. The model order reduction techniques are applied to the obtained autopilots at different design trials and the obtained results clarify that the multiplicative method yields better results and consequently it is used forward in this work.

4.2.2 Autopilot Robustness Evaluation

Un-modelled Dynamics: The five designed controllers are implemented at the remainder operating points. The results clarify that the controller obtained taking the 6th operating point as a nominal transfer function (Case-A) is not robust against all unmodeled dynamics with the 1st and 2nd controllers in the early operating points while it is robust against all unmodeled dynamics for the third controller (Trial-3) but with slower response. On the other hand the controller obtained taking the 4th operating point (Case-B) as a nominal transfer function is robust against all unmodelled dynamics but with slower response than that obtained with Case-A especially in the final operating points. These results are summarized in Fig. 13, which clarifies that the controller C_{A2} which has smallest values of $\|\omega_p S\|_\infty$ and $\|\omega_t T\|_\infty$ has faster response than C_{A1} and C_{A3}. However, the obtained controller have a large control effort at the beginning of action with lowest values at steady state compared to original controller as shown in Fig. 14.

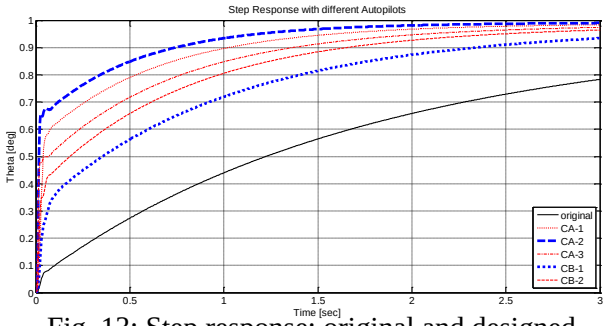

Fig. 13: Step response: original and designed

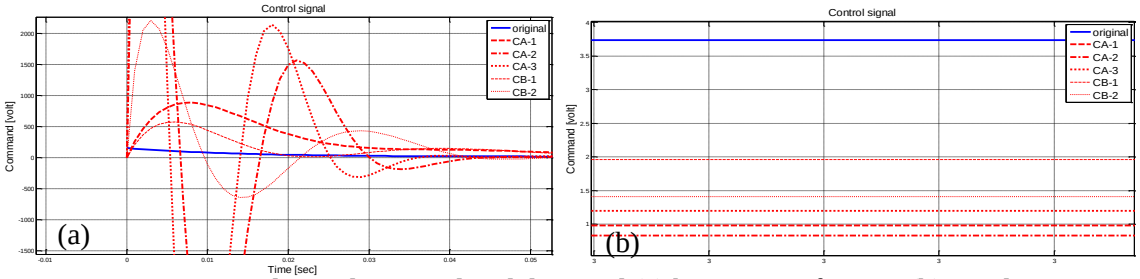

Fig. 14: Control signal: original and designed (a) beginning of action (b) steady state

Noise Attenuation

Applying noise on the gyro output the obtained control effort is shown in Fig. 15, which clarify that C_{A1} and C_{B1} which have $\|\omega_t T\|_\infty$ >1 is less sensitive to additive noise compared to other controllers.

Disturbance Rejection

Applying a disturbance on the jetivator output, the obtained closed loop step response is shown in Fig. 16 which clarifies that the controller C_{A2} is the best compared to other controllers as it rejects 50% within 0.1 [sec] and 95% within 0.5 [sec]. Also control effort is shown in Fig. 17 which reveals that this controller has the lowest control effort after applying the disturbance. These results clarify that the designed robust controllers C_{A1} and C_{A2} is less sensitive to noise and disturbance and consequently they have the lowest control effort, but they are not robust against unmodelled dynamics in the early operating conditions.

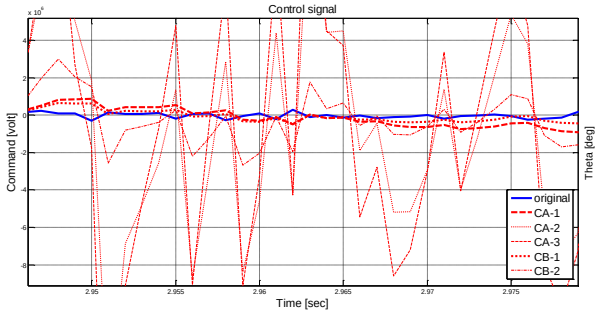

Fig. 15: Control signal: original and designed

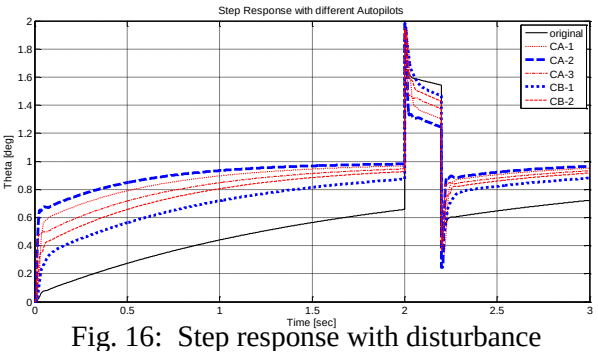

Fig. 16: Step response with disturbance

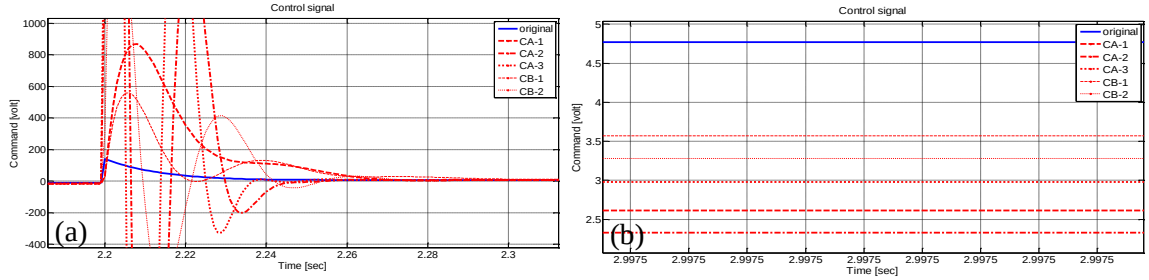

Fig. 17: Control signal: original and designed (a) beginning of action (b) steady state

4.3 Autopilot Synthesis with Uncertainty Modelling

This section is devoted to the design of a robust system for attitude/horizontal stabilization of a time-varying thrust vector control. The linearized equations of the longitudinal motion are derived with the consideration of variations in the aerodynamic coefficients as parametric uncertainties in the design such that the desired closed-loop performs in the presence of uncertainty, disturbances and noises. Robust stability and robust performance of the closed-loop system with the implementation of each controller are investigated.

4.3.1 Pitch Plane Performance Requirements

The stabilization channel is to achieve and maintain the desired body angle in the presence of uncertainties. A block-diagram of the closed-loop system including the feedback and controller as well as the elements reflecting the model uncertainty and weighting functions related to performance requirements is shown in Fig. 18. This system has a reference signal r and two weighted outputs e_p and e_u which characterize performance requirements. The transfer function W_g represent the free gyro dynamics that measures θ. The system M is the ideal model to be matched by the designed closed loop system. The rectangular box, shown with dotted line, represents the perturbed plant model $G = F_u(G_{mis}, \Delta)$, where G_{mis} is the nominal model of the rocket and Δ parameterizes the model uncertainty. The matrix Δ is unknown but has a diagonal structure and is norm bounded, i.e. $\|\Delta\|_\infty$ <1. For robust

performance, it is required that the transfer function matrix from r to e_p and e_u should be small in the sense of $\|.\|_\infty$, for all possible uncertain matrices Δ. The transfer function matrices W_p and W_u are employed to represent the relative significance of performance requirements over different frequency ranges. The measured output feedback signal is $y = W_g\theta$ and the gyro transfer function is chosen as $W_g = \frac{0.044}{0.022s+1}$. That is, the synthesis problem of the missile attitude stabilization system is to find a linear, stabilizing controller C(s), with feedback signals y to ensure the required properties of the closed-loop system.

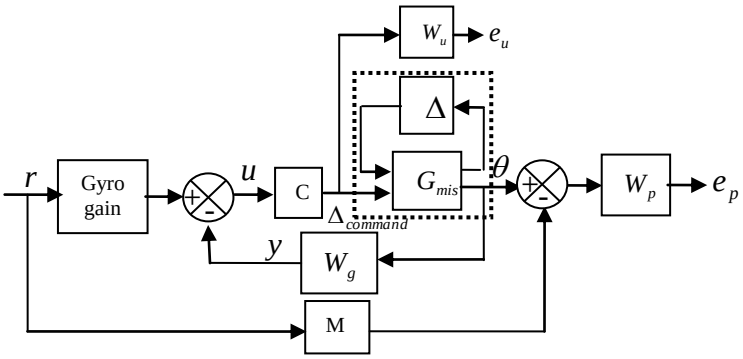

Fig. 18 The closed loop system with perturbation

Nominal performance: The closed-loop system achieves nominal performance where the perturbation matrix Δ is zero. Let us denote by $\phi = \phi(G,C)$ be the transfer function of the closed-loop system from r to e_p and e_u, $\begin{bmatrix} e_p(s) \\ e_u(s) \end{bmatrix} = \phi(s)[r(s)]$. The criterion for nominal performance is to satisfy the inequality $\|\phi_{mis}(s)\| < 1$ where $\phi_{mis}(s)$ is the transfer function matrix of the closed-loop system for the case Δ=0. This criterion is a generalization of the mixed sensitivity optimization problem and includes performance requirements by matching an ideal system M.

Robust Stability: The closed-loop system achieves robust stability if the closed-loop system is internally stable for all possible, perturbed plant dynamics $G = F_u(G_{mis}, \Delta)$.

Robust Performance: The closed-loop system must remain internally stable for each $G = F_u(G_{mis}, \Delta)$ and, in addition that the performance criterion $\|\phi(s)\|_\infty < 1$ must be satisfied for each $G = F_u(G_{mis}, \Delta)$.

The ideal system model to be matched with and satisfies the requirements to the closed-loop dynamics is chosen as $M = \frac{100^2}{s^2 + 80s + 100^2}$ and the performance weighting functions are $W_p(s) = \frac{0.1s+5}{3s+0.015}$ and $W_u(s) = \frac{0.4s+0.9}{5.9s+5}$. The performance weighting functions are chosen so as to ensure an acceptable trade off between the nominal performance and robust performance of the closed-loop system with control action which satisfies the constraint imposed. The frequency response of the inverse of performance weighting function W_p^{-1} is shown in Fig. 19 which clarifies that over the low frequency range it is required to have a small difference between the system and model and small effect on the system output due to disturbances. This ensures good reference tracking and small error in the case of low-frequency disturbances.

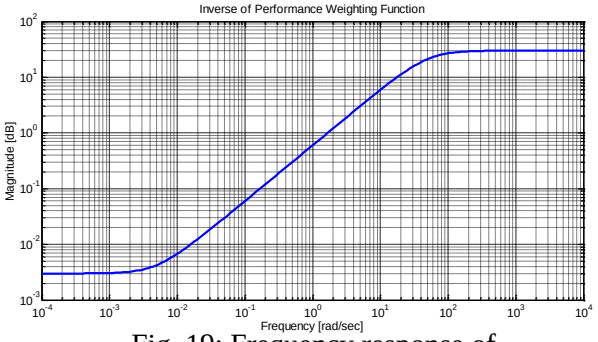

Fig. 19: Frequency response of the inverse weighting function

The internal structure of the open loop interconnection for the missile stabilization system with 7 inputs and 8 outputs is shown in Fig. 20a, where the open loop system is of 10^{th} order. The reference signal is the variable (ref), the control action is the variable control (u) and the measured output is the variable (y). A schematic diagram showing the specific input/output ordering for the system variables is shown in Fig. 20b. Consider the 6^{th} operating point as a nominal transfer function (Case-A) with the previous weights from which the designed controller obtained is of 10^{th} order. The frequency response of the structured singular value (μ) for the case of robust stability analysis is shown in Fig. 21, where the maximum value of structured singular value $\mu_{max} = 0.47578$, which means that the stability of the closed-loop system is preserved under all perturbations that satisfy $\|\Delta\|_\infty < \frac{1}{0.47578}$.

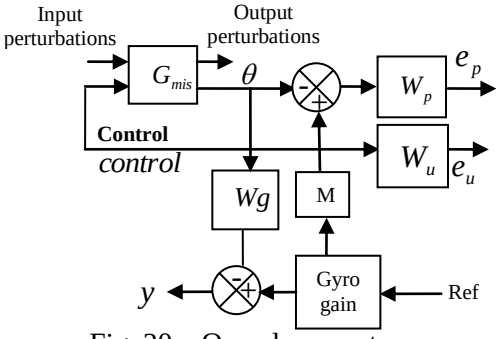

Fig. 20a: Open loop system with performance requirements

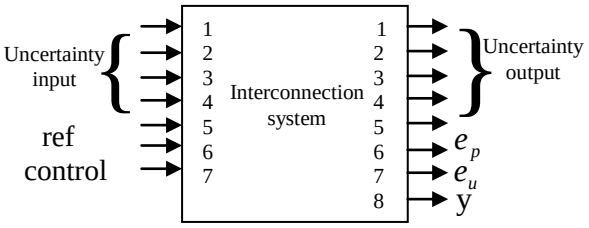

Fig. 20b: Open-loop system schematic

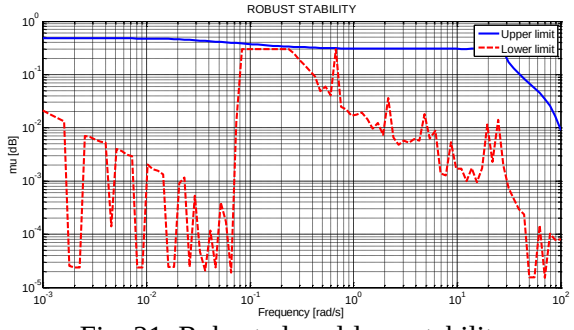

Fig. 21: Robust closed-loop stability

The nominal performance of the closed loop system transfer matrix is tested via the frequency response as shown in Fig. 22. The obtained peak value of γ is 2.5863 which is not less than 1 and shows that the nominal performance has not been achieved. The robust performance of the closed-loop system with the uncertainty matrix Δ using the H_∞ controller is also

investigated by means of the μ analysis. The robust performance (in respect to the uncertainty and performance weighting functions) is achieved if and only if, over a range of frequency under consideration, the structured singular value $\mu_{\Delta_p}(j\omega)$ at each ω is less than 1. The frequency response of μ for the case of robust performance analysis is given in Fig. 23, where the peak value of μ is 3.2273, which shows that the robust performance has not been achieved. In other words, the system does not preserve performance under all relative parameter changes.

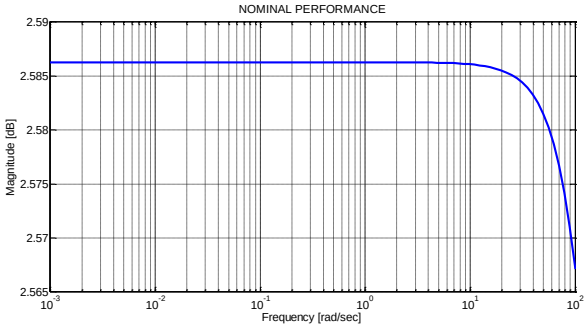

Fig. 22: Nominal closed-loop performance

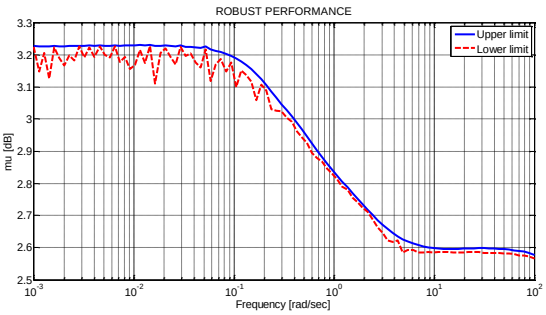

Fig. 23: Robust closed-loop performance

To check if the designed controller achieves robust stability and robust performance of the closed-loop system at other time instants of flight, further analysis should be conducted with corresponding dynamics. The closed loop simulation is conducted via a program designed and corresponds to the structure shown in Fig. 24, in which the performance weighting functions W_p and W_u are absent. The simulation shows the transient responses of the closed loop system with the designed H_∞ controller for a step command is shown in Fig. 25, where the system is under damped with accepted characteristics.

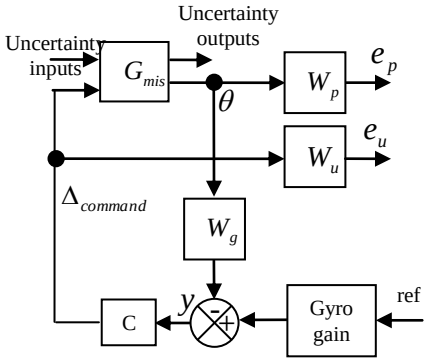

Fig. 24: Closed loop Structure

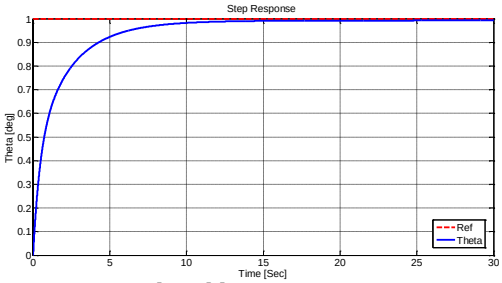

Fig. 25: Closed loop transient response

The singular value plot of closed loop poles is shown in Fig. 26, which reveals that there exist some singular values > 1 and that the H_∞ norm of the closed loop system is greater than 1, i.e. the condition $\left\|W_p(I+GC)^{-1}\right\|_\infty < 1$ is not satisfied in this case.

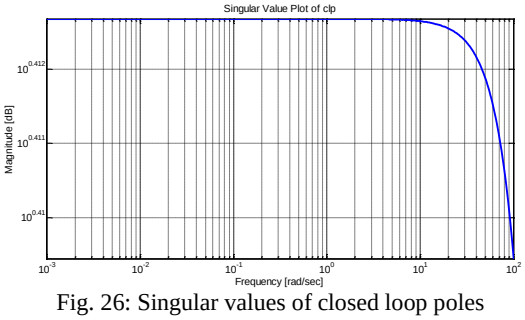

Fig. 26: Singular values of closed loop poles

Redesign the robust controller using the following performance weighting functions $W_p(s) = \frac{0.1s + 5}{27.2522s + 0.015}$ and $W_u(s) = \frac{0.4s + 0.9}{5.9s + 5}$ at the same operating point which results in a controller of $10^{\underline{th}}$ order. The frequency response of the structured singular value for the case of robust stability analysis is considered, where μ_{max} = 0.47705, which means that the stability of the closed-loop system is preserved under all perturbations that satisfy $\|\Delta\|_\infty < \frac{1}{0.47705}$. From the frequency response of the nominal performance it is seen that the obtained peak value of γ is 1.001 and less than 1 in the high frequency range which shows that the nominal performance has achieved. In addition, the peak value of μ is 1.6, and less than 1 in the high frequency range which shows that the robust performance has achieved. That is, the system does preserve performance under all relative parameter changes. The transient response of the closed loop system with the designed H_∞ controller for a step command is obtained, where the system is under damped with accepted characteristics. The singular value plot of closed loop poles reveals that all singular values < 1 which show that the H_∞ norm of the closed loop system is less than 1, and the condition $\left\|W_p(I + GC)^{-1}\right\|_\infty < 1$ is satisfied in this case.

4.3.2 Yaw Plane Performance Requirements

The performance weighting functions are $W_p(s) = \frac{0.1s + 4.261}{18.5s + 0.02}$ and $W_u(s) = \frac{0.4s + 0.9}{5.9s + 5}$ from which the designed controller obtained is of $10^{\underline{th}}$ order. For the case of robust stability analysis, the maximum value of structured singular value μ_{max}= 0.40335, which means that the stability of the closed-loop system is preserved under all perturbations that satisfy $\|\Delta\|_\infty < \frac{1}{0.40335}$. The nominal performance of the closed loop system transfer matrix is tested via the frequency response. The obtained peak value of γ is 1.0009 and less than 1 at high frequency range which shows that the nominal performance has been achieved. For the case of robust performance analysis, the peak value of μ is 1.5821, and less than 1 at high frequency which shows that the robust performance has been achieved. In other words, the system does preserve performance under all relative parameter changes with uncertainty range (25 %). The simulation shows the transient responses of the closed loop system with the designed H_∞ controller for step command where the system is under-damped with accepted characteristics. The singular value plot of closed loop poles is considered, which reveals that all singular values < 1 and that the H_∞ norm of the closed loop system is less than 1, i.e. the condition $\left\|W_p(I + GC)^{-1}\right\|_\infty < 1$ is satisfied in this case. Note that, the model order reduction techniques are applied to the obtained controller using multiplicative method and yields 4^{th} order autopilots.

4.3.3 Autopilot Robustness Evaluation

Unmodeled Dynamics

The two designed controllers in pitch plane and the designed controller in yaw plane are implemented at the different operating points, two (early and final operating points) for each are illustrated in Fig. 27, which clarify the robustness of these designed controllers against all unmodelled dynamics.

The results are summarized in Fig. 28a and clarify that the designed robust controllers with uncertainty modeling has faster response than those designed without modeling the uncertainty and the classical one. In addition, the obtained robust controller with uncertainty

modeling have a lowest control effort at the steady state compared to others as shown in Fig. 28b,c which illustrate the fast Fourier transform spectrum of the control signal and reveal that the control effort obtained via designed robust controllers with uncertainty modeling has a lowest band of operating frequencies.

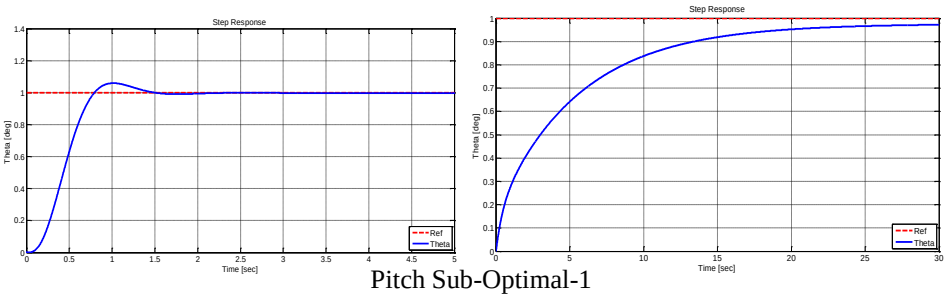

Pitch Sub-Optimal-1

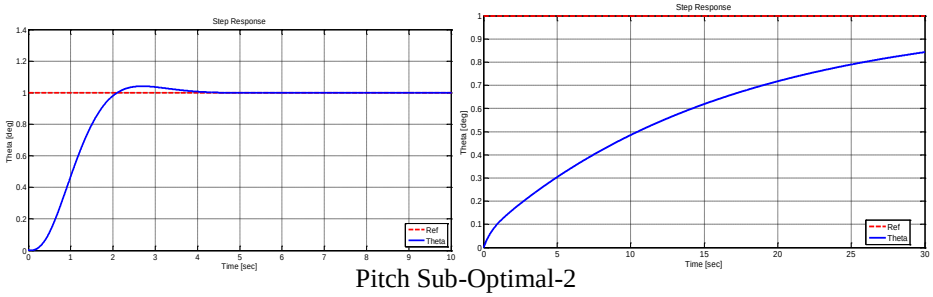

Pitch Sub-Optimal-2

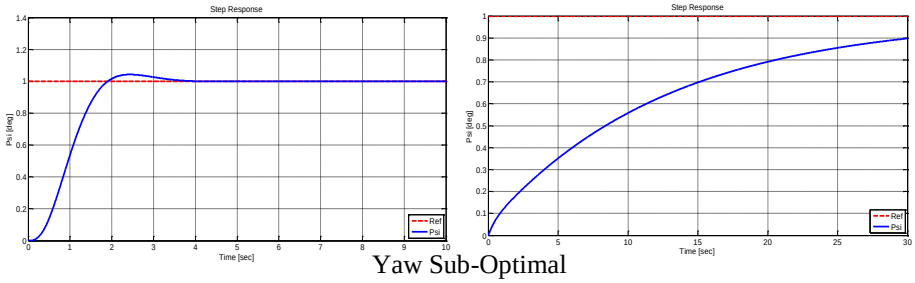

Yaw Sub-Optimal

Fig. 27: Closed loop Step response

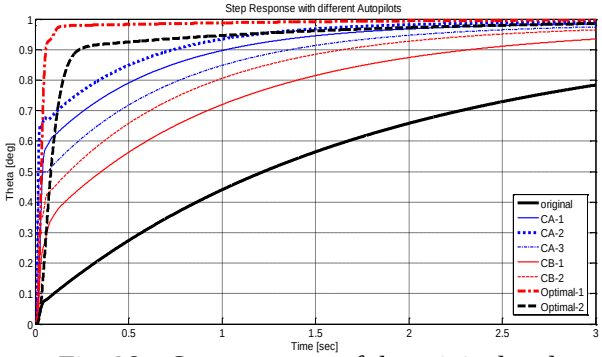

Fig. 28a: Step response of the original and designed controller

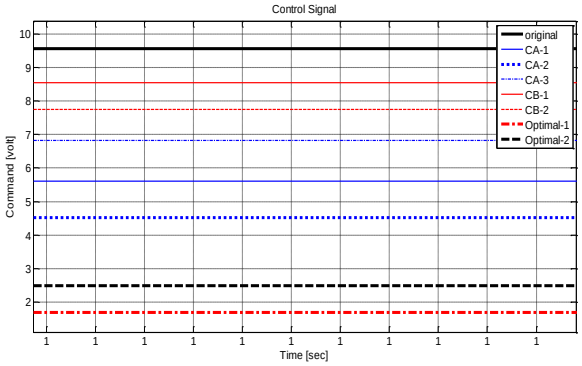

Fig. 28b: Control signal of the original and designed controller

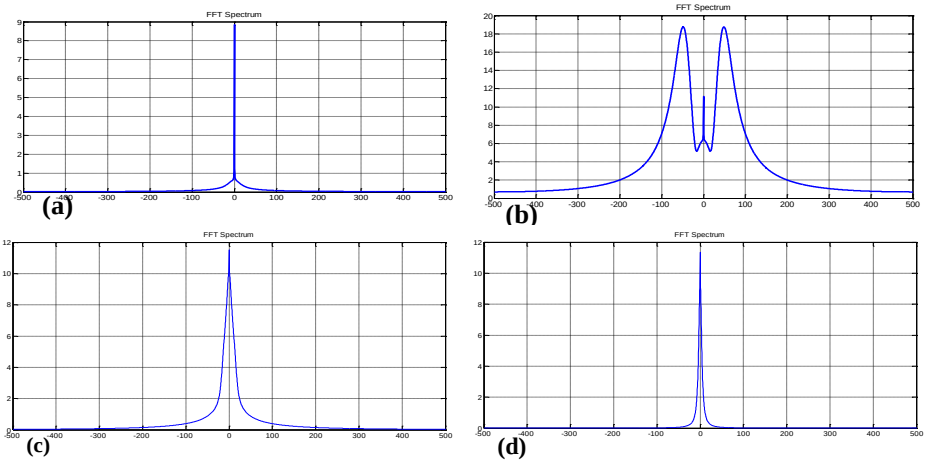

Fig. 28c: FFT (a) original (b) C_{A2} (c) Optimal-1 (d) Optimal-2 controllers

Noise Attenuation

Applying noise to the gyro output the obtained control effort is shown in Fig. 29a,b which clarify that the designed robust controller with uncertainty modeling is less sensitive to additive noise compared to other controllers.

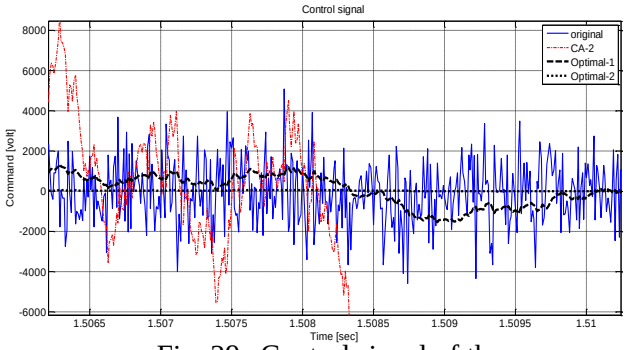

Fig. 29a Control signal of the original and obtained controller

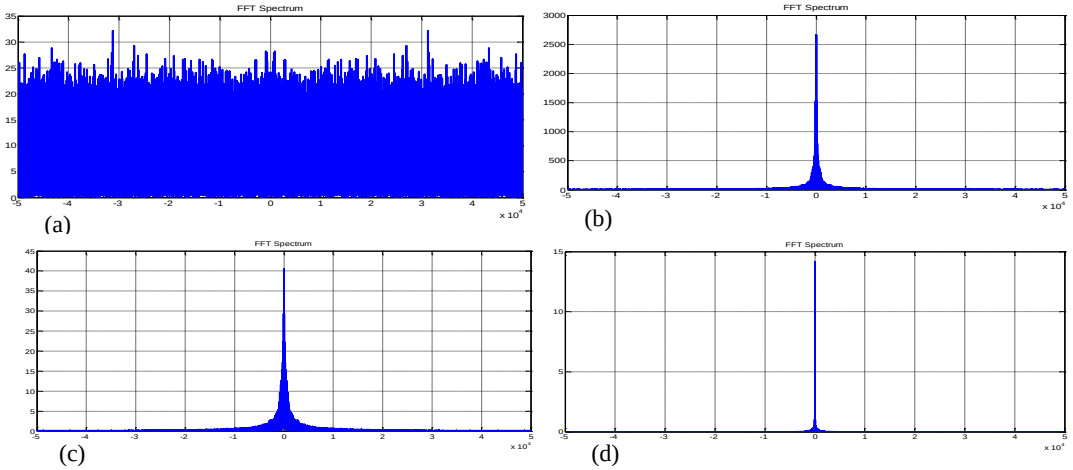

Fig. 29b: FFT of (a) original (b) C_{A2} (c) Optimal-1 (d) Optimal-2 controllers

Disturbance Rejection

Applying disturbance on the jetivator output the obtained step response of closed loop system is shown in Fig. 30a which clarifies that the designed robust controllers with uncertainty modelling is the best compared to other controllers as it rejects 50% within 0.1 sec and 95%

within 0.25 sec. Also the control effort shown in Fig. 30a,b reveals that this autopilot has the lowest steady state control effort.

The same evaluation of yaw plane clarifies that the designed robust controllers with uncertainty modeling has faster response a lowest steady state control effort than classical one and the obtained robust controller without modeling the uncertainty. In addition, applying noise clarify that designed robust controllers with uncertainty modeling is less sensitive to additive noise compared to others. Also the response results to disturbance on the jetivator output clarify its capability reject 50% within 0.09 sec and 95% within 0.22 sec.

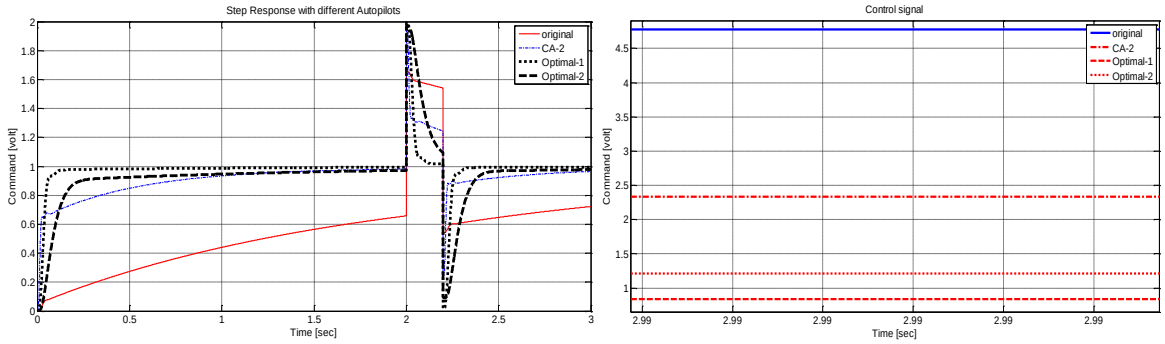

Fig. 30a: Step response and control signal of original and designed controllers

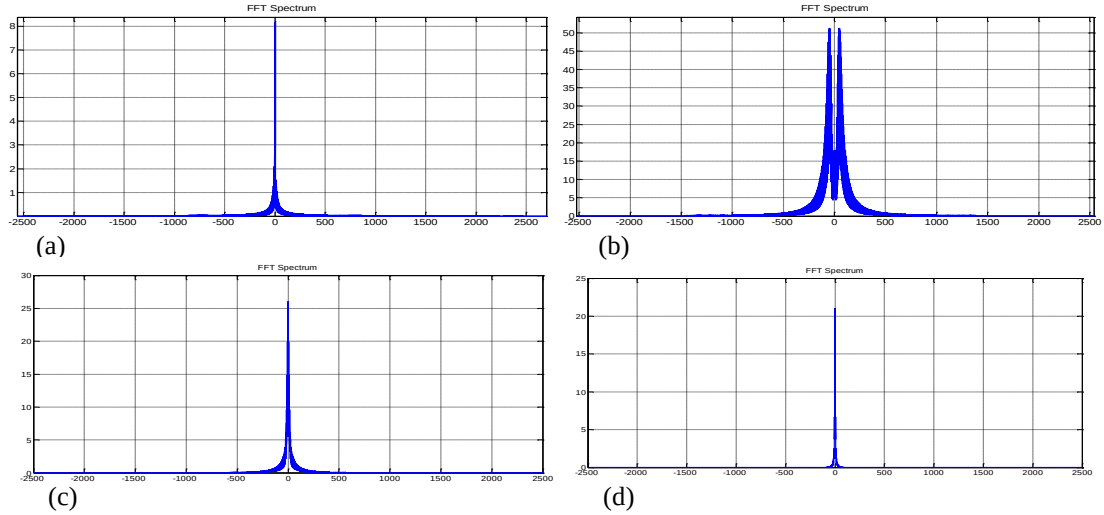

Fig. 30b: FFT of (a) original (b) C_{A2} (c) Optimal-1 (d) Optimal-2 controllers

Flight Path Evaluation

The obtained controllers are evaluated with the flight path trajectory at the minimum and maximum tactical data (500 [m]), (2800 [m]), respectively, at different flight conditions. For simplicity a sample of obtained results is shown.

Thrust Variation: The designed autopilots are evaluated with the flight path against classical autopilot and using different thrust values as shown in Fig. 31a-b.

The robust autopilot proved its robustness to thrust uncertainties to about 30% degradation with little oscillation at the gathering phase compared to nominal thrust case.

Variation in Aerodynamic coefficients: The designed autopilots are evaluated against perturbations in the aerodynamic coefficients of about ±30% and the results are shown in Fig. 32a-b.

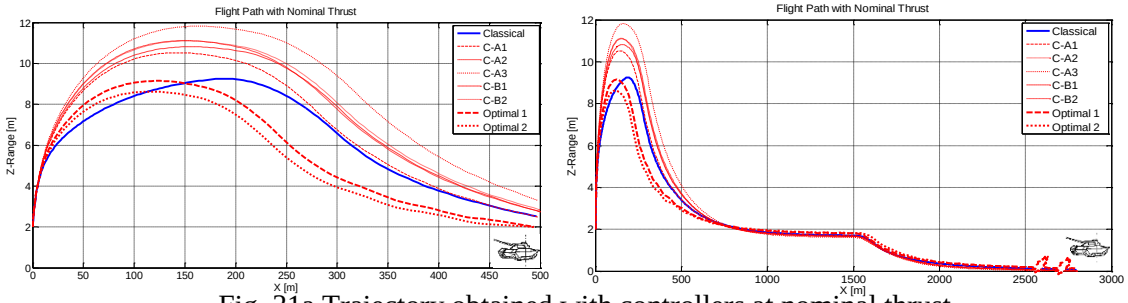

Fig. 31a Trajectory obtained with controllers at nominal thrust

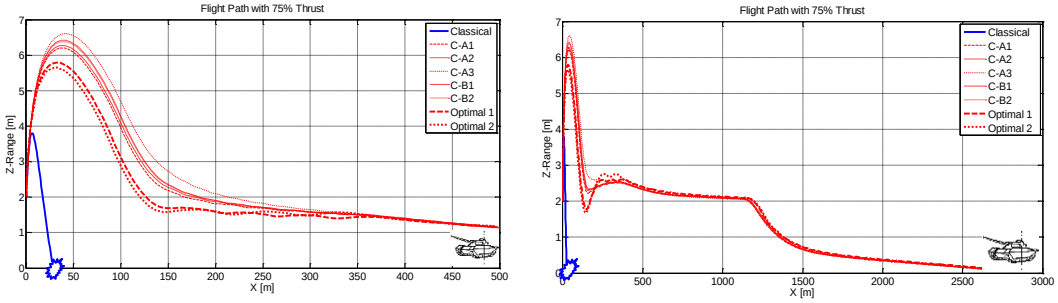

Fig. 31b Trajectory obtained with controllers at 75% thrust

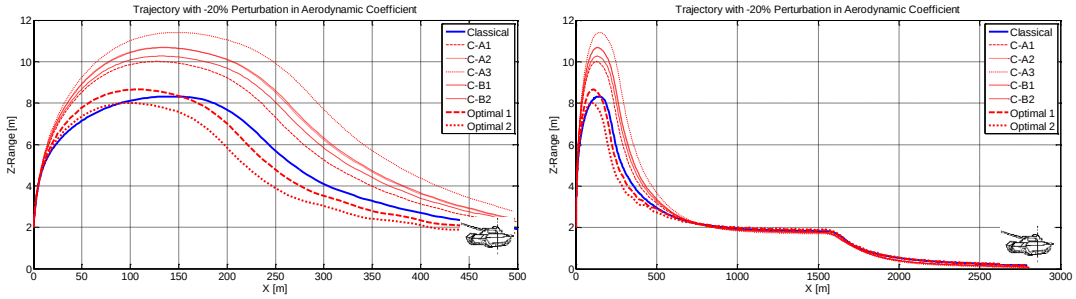

Fig.32a: Trajectory with -20% variations in aerodynamic coefficients

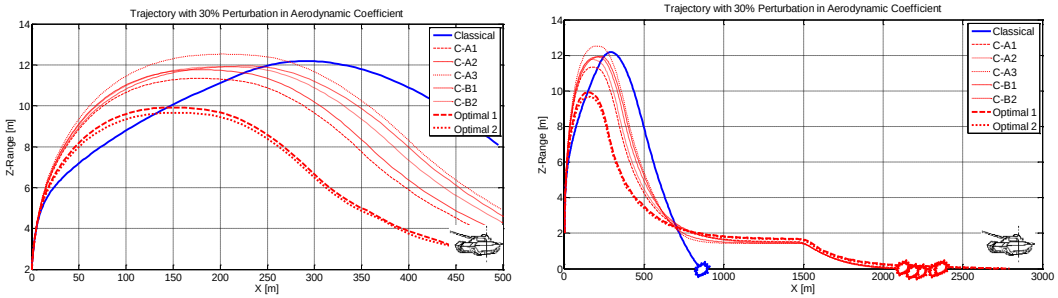

Fig. 32b: Trajectory with 30% variations in aerodynamic coefficients

The results obtained with varying aerodynamics clarify that the robustness of designed autopilots without uncertainty modeling is limited to about 5% to -20% of nominal values

after which the missdistance will be large or missile ground impact occurs. While the robustness of designed autopilot, with uncertainty modeling, is limited to about ±30% of nominal value.

Wind Speed in X Direction: The simulation is conducted with considering the wind speed along the X-axis from which the results are shown in Fig. 33a-b.

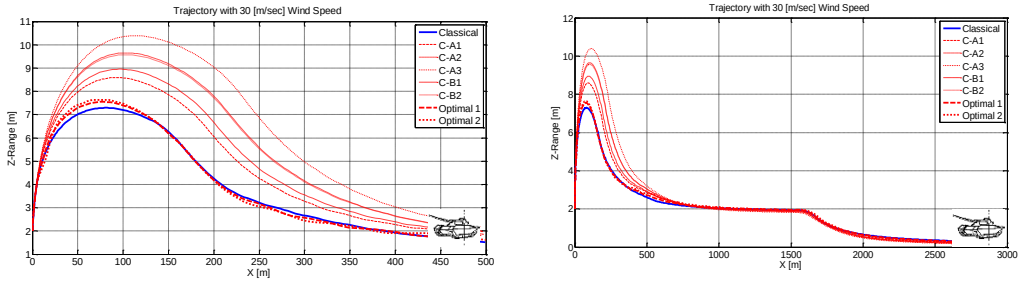

Fig. 33a: Trajectory with $V_{w_x} = 30[m/\sec]$

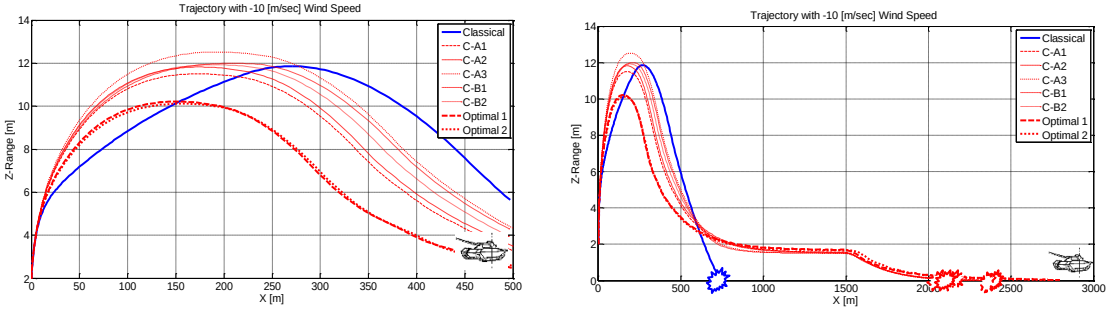

Fig. 33b: Trajectory with $V_{w_x} = -10[m/\sec]$

The results obtained with considering wind velocity along the X-axis clarify that the robustness of designed autopilots without uncertainty modeling is limited to about -5:30 [m/sec], while the robustness of designed autopilots with uncertainty modeling is limited to about -19:30 [m/sec].

Wind Speed in Y Direction: The simulation is conducted with considering the wind speed along the Y-axis from which the results are shown in Fig. 34a-b.

The results obtained with considering wind velocity along the Y-axis clarify that the robustness of designed autopilots with uncertainty modeling is limited to about ±30 [m/sec], while the designed robust autopilots without uncertainty modeling is limited to about ±15 [m/sec].

Wind Speed in Z Direction: The simulation is conducted with considering the wind speed along the Z-axis from which the results are shown in Fig. 35a-b. The results obtained with considering wind velocity along the Z-axis clarify that the robustness of designed autopilots with uncertainty modeling is limited to about ±20 [m/sec], while the designed robust autopilots without uncertainty modeling is limited to about -20:15 [m/sec].

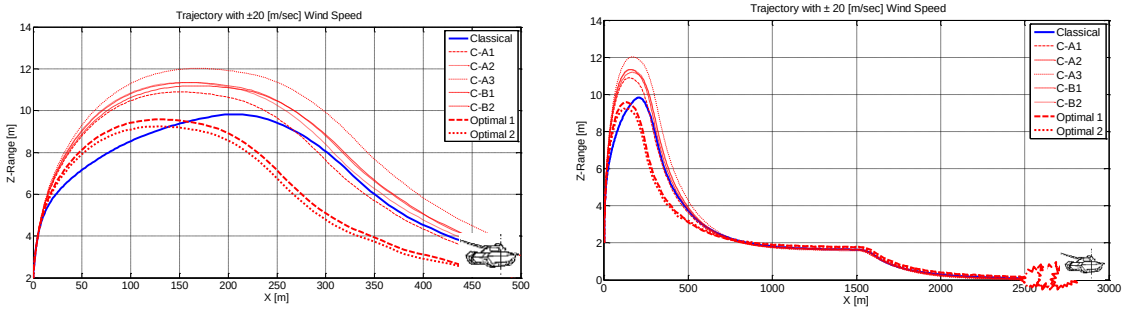

Fig. 34a: Trajectory with $V_{w_y} = \pm 20 [m/\sec]$

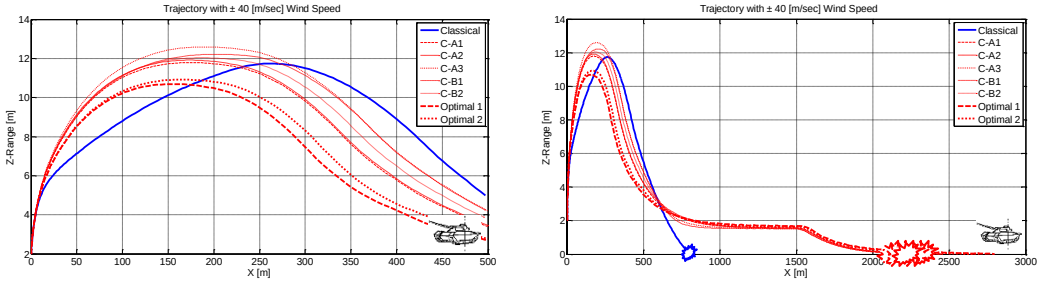

Fig. 34b: Trajectory with $V_{w_y} = \pm 40 [m/\sec]$

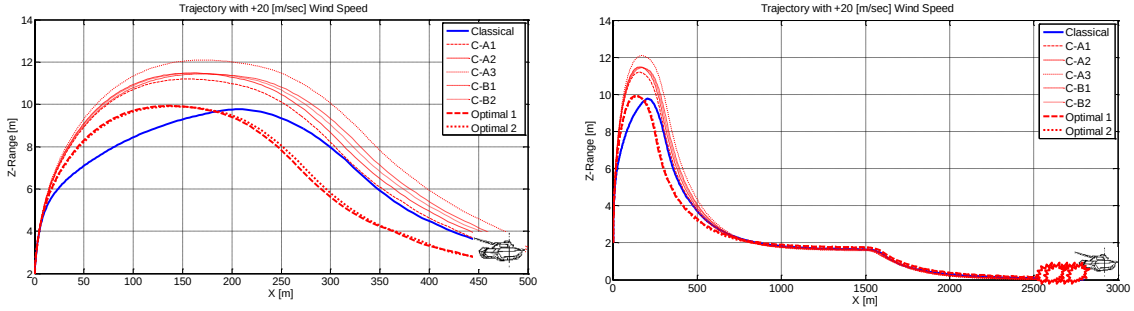

Fig. 35a: Trajectory with $V_{w_z} = +20 [m/\sec]$

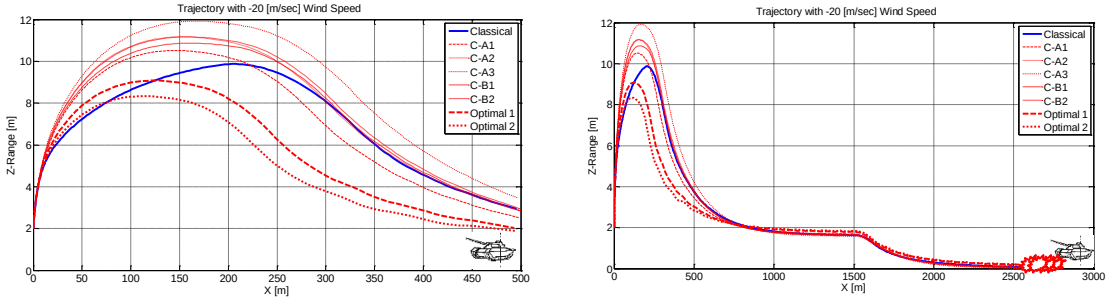

Fig. 35b: Trajectory with $V_{w_z} = -20 [m/\sec]$

The results obtained reveal that the designed robust controller with uncertainty modelling which satisfy the equality $\left\| W_p (I + GC)^{-1} \right\|_\infty < 1$ (sub-optimal2) is the best design. This controller proves its robustness against un-modelled dynamics, stable flight path with the consideration of different sources of uncertainties (thrust degradation, aerodynamic coefficient variation and wind speed), low miss-distance, low control effort, and less sensitivity to additive noise and disturbance. The remainder designed autopilots are sorted in a

descending order from the best performance to lowest one as: sub-optimal1, C_{A2}, C_{A1}, C_{B2}, C_{B1}, C_{A3} and finally the classical autopilot.

5. Flight Performance Evaluation

The obtained sub-optimal controllers in both pitch and yaw planes are evaluated via the flight path trajectory at different flight scenarios with existence of additive random noise applying on the measuring devices (gyros).

5.1 Thrust Variation with Measurement Noise

The 6DOF simulation is conducted with target at 2800 [m] (500 [m]) and separated from line of sight in yaw plane with angle $\psi_s = 2.8^o$ at thrust (nominal - 90% - 85%) values and additive noise on pitch and yaw gyros. The additive noise is shown in Fig. 36a and its influence on gyros outputs are shown in Fig. 36b,c,d. The flight path trajectories are shown in Fig. 37.

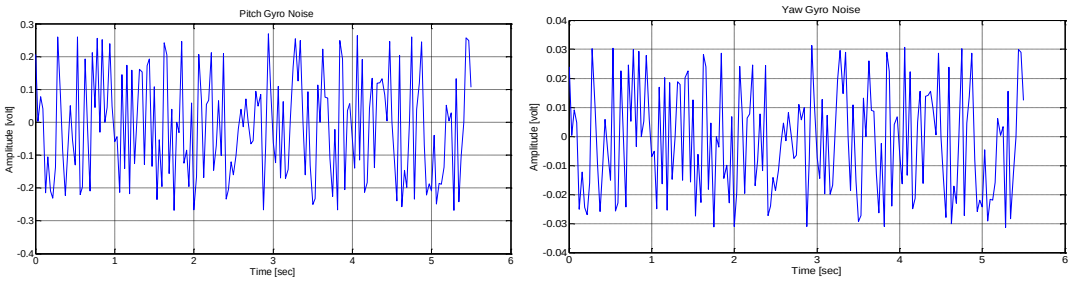

Fig. 36a: Additive noise on pitch and yaw gyros

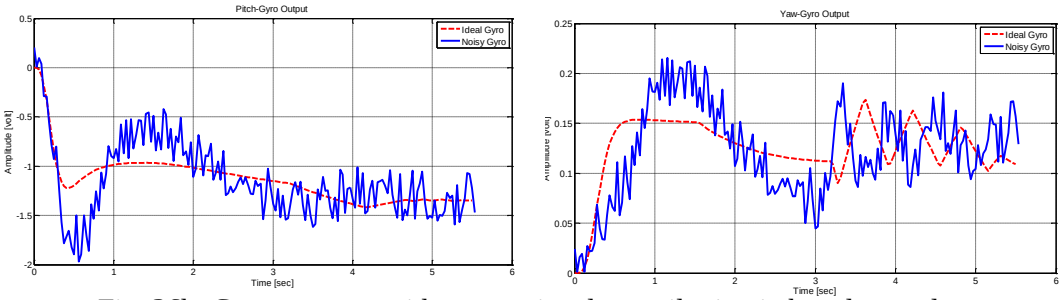

Fig. 36b: Gyros outputs with conventional autopilot in pitch and yaw planes

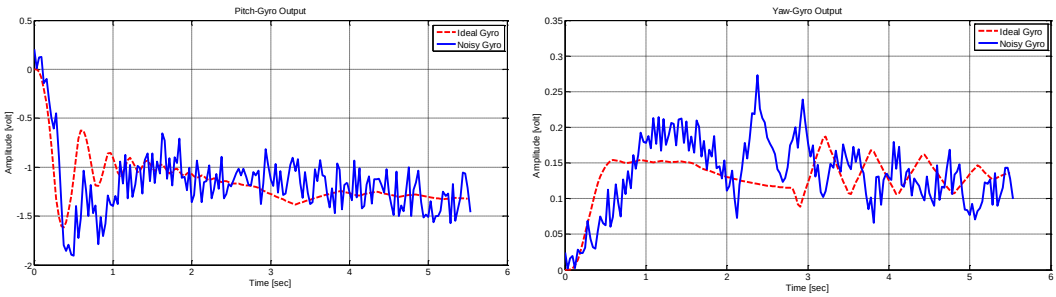

Fig. 36c: Gyros outputs with optimal pitch autopilot and conventional yaw autopilot

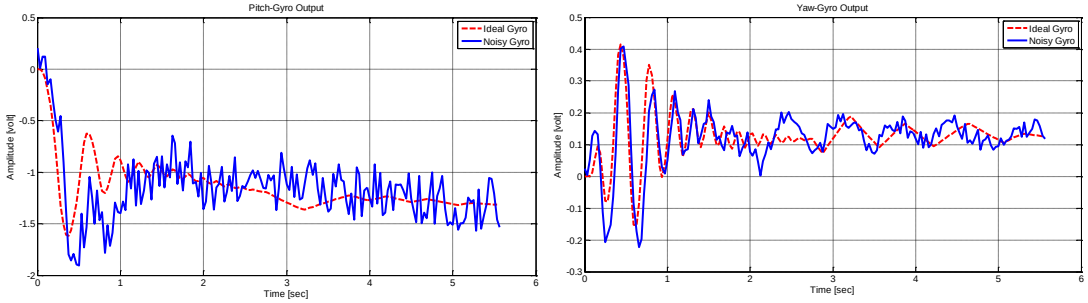

Fig. 36d: Gyros outputs with optimal autopilot in pitch and yaw planes

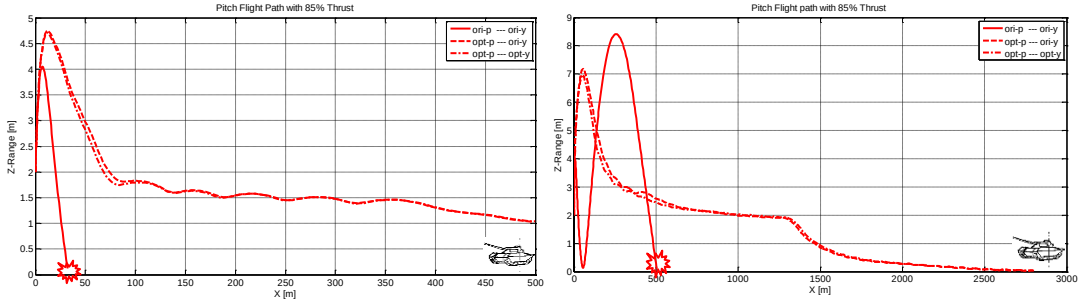

Fig. 37: Pitch Trajectory with controllers at 85% thrust

These results reveal that the optimal autopilot has the least sensitivity to measurement noise in addition that the conventional autopilot has less stable trajectory compared to the optimal one. The miss-distance [m] is summarized as follows:

Range [m]	Thrust [%]	Conventional-pitch Conventional-yaw	Optimal-pitch Conventional-yaw	Optimal-pitch Optimal-yaw
500	100	2.3174	3.329	2.2893
	90	2.1433	3.414	1.2436
	85	Ground impact	2.733	1.2086
2800	90	0.9317	1.596	0.8417
	85	Ground impact	1.78	0.4254

5.2 Effect of Yaw Separation Angle (ψ_s)

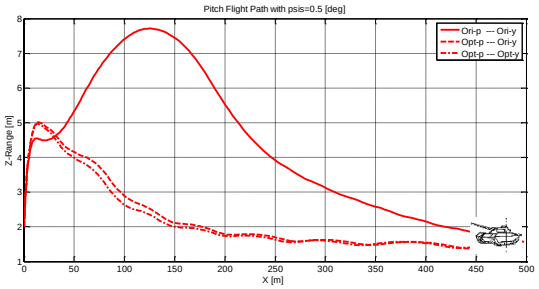

Fig. 38: Pitch Trajectory with autopilots at $\psi_s = 0.5^o$

The 6DOF simulation is conducted using the target distance at 500 [m] and separated from line of sight in yaw plane with angle ($\psi_s = 1.5^o$, $\psi_s = 1^o$, $\psi_s = 0.5^o$ (9mils)) at 90% thrust values and additive noise on pitch and yaw gyros. The sample influence of the measurement noise on

the flight path trajectories is shown in Fig. 38. The results reveal that the conventional autopilot has less stable trajectory compared with the optimal one and the miss-distance [m] is summarized as follows:

ψ_s [deg]	Conventional-pitch Conventional-yaw	Optimal-pitch Conventional-yaw	Optimal-pitch Optimal-yaw
1.5^o	2.0569	2.9406	1.1713
1^o	1.9040	2.7252	1.1600
0.5^o	1.9520	2.9014	1.7157

5.3 Effect of Target Motion

In this case outgoing / incoming target with average speed V_T = 65 [Km/hr] and range 2800 [m] (500 [m]) is considered. In addition, the LOS separation angle in Yaw plane is $\psi_s = 2.8^o$ ($\psi_s = 0.5^o$) without measurement noise and at nominal thrust value. The 6DOF simulation is conducted using the designed autopilots from which the flight path trajectories are shown in Fig. 39.

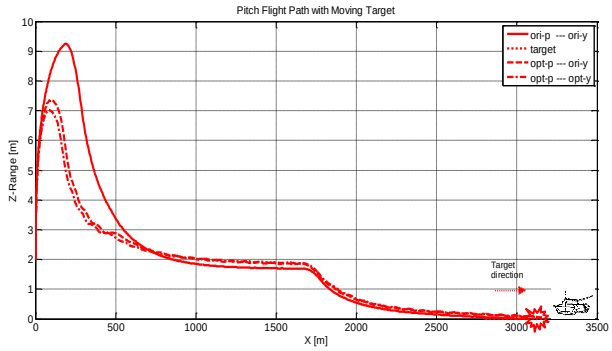

Fig. 39a: Pitch Trajectory with outgoing target

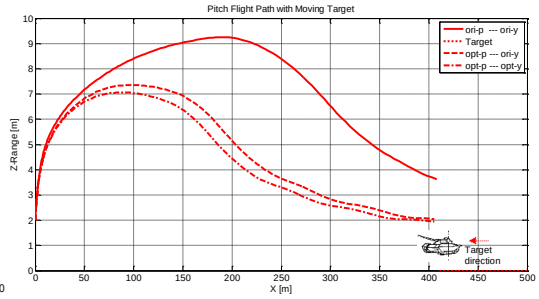

Fig. 39b: Pitch Trajectory with incoming target

These results reveal that the sub-optimal autopilots have successful engagements against outgoing / incoming targets and the miss-distance [m] is summarized as follows:

Range [m]	Target	Conventional-pitch Conventional-yaw	Optimal-pitch Conventional-yaw	Optimal-pitch Optimal-yaw
3000	Outgoing	ground impact	1.038	1.1782
	Incoming	0.4180	0.754	0.6466
500	Outgoing	1.6183	1.3756	1.4593
	Incoming	3.6435	2.04	2.2389

6- Conclusion

This paper presented the robust control theory in the form of two approaches; the H_∞ and sub-optimal H_∞ designs with different sensitivities and norms. In addition, it presented the model reduction techniques that can be utilized for reducing the controller order. Then, the underlying system is formulated in structures appropriate for utilizing these design techniques. The autopilots designed using the two techniques are evaluated against stability, un-modeled dynamics, disturbance rejection, noise attenuation and flight path. The obtained

results clarify that the sub-optimal H_∞ controller, where the uncertainties are modeled during the design process, is more robust than the other H_∞ technique, where the design process is carried out without modeling the uncertainties, and the classical one. These autopilots proved its robustness to thrust uncertainties within ±30% degradation, and about ±30% of nominal aerodynamic coefficients. In addition, it is limited to wind speed of about V_{wx} = -19:30 [m/sec], V_{wy} =±30 [m/sec], and V_{wz}=±20 [m/sec]. It proved its capability of faster response with the lowest steady state control effort, less sensitivity to measurement noise and reject disturbance of 50% within 0.09 sec and 95% within 0.22 sec.

7- References

[1] Astrom, K. J., *Model Uncertainty and Robust Control*, Department of automatic control Lund University, Lund, Sweden.

[2] Bryant, G.F. and G. D. Halikas, *Optimal Loop-Shaping for Systems With Large Parameter Uncertainty Via Linear Programming*, Int. J. control,1995,Vol. 62, No.3, 557-568.

[3] Cashmore, R.D., G.D.Halikias and D.A.Wilson, *Adaptive and Robust Control of a Flexible Manipulator System* .

[4] Da-Wei Gu, Petko H. Petkov and Mihail M. Konstantinov, *Robust Control Design With Matlab*,

[5] Dolye, Bruce Francis, Allen Tannenbaum, *Feedback Control Theory*, Macmillan Publishing Co., 1990.

[6] El-sheikh, G.A., *Theory of Guidance and Systems*, (2000).

[7] El-sheikh, G.A., *Novel Derivation for the Polynomial Optimal Control Methods. LQG Controller Design*, Cairo, 1997.

[8] El-sheikh, G.A., *On H_∞ Self-Tuning Control and its Aerospace Applications*, Ph.D. Thesis, Industrial control centre, University of Strathclyde, U.K., 1994.

[9] Garnell P. and East D. J., *Guided Weapon Control Systems*, 2nd edition, pergamon precs, New York, (1980).

[10] Glover, K., *All Optimal Hankel Norm Approximation of Linear Multivariable Systems*, Int. J. Control, Vol. 39, no. 6, pp. 1145-1193, 1984.

[11] Kwakernaak H., *Robust Control and H_∞ Optimization*, Tutorial Paper, Automatica, Vol.29, No.2, pp 255-273, 1993.

[12] looye, G. ,A.varga , s.bennani , D.moormann , G.grubel, *Robustness Analysis Applied to Autopilot Design*,

[13] Maintenance and Repair Documents of the swing fire missile.

[14] Math Works, Inc., *Robust Control Toolbox User's Guide*, copyright 1992 – 2001.

[15] Menona, P.K. , E.J. Ohlmeyerb *Integrated Design of Agile Missile Guidance and Autopilot Systems*,*Control Engineering* Practice 9 (2001) 1095–1106

[16] Michael Anderson, Michael Buehner, Peter Young, Douglas Hittle, Charles Anderson, Jilin Tu, and David Hodgson, *MIMO Robust Control for HVAC Systems*, IEEE Transactions On Control Systems Technology, Vol. 16, No. 3, MAY 2008.

[17] Oda, A.N. , G.A. El-Sheikh, Y.Z. El-Halwagy and M. Al-Ashry *Robust CLOS Guidance and Control Part-1: System Modeling and Uncertainty Evaluation*,14th International Conference on Aerospace Sciences & Aviation Technology,2010.

[18] Paulo C. Pellanda , Pierre Apkarian ,Hoang Duong Tuan ,Daniel Alazard, *Missile Autopilot Design Via A Multi-Channel LFT/LPV Control Method*,

[19] Stefani, R.T., Savant, C.J., Shahian, B. and Hostetter, G.H., *Design of Feedback Control System*, Third Edition, Saunders College Publishing, 1994.